Experimental Observation of Temporal Pumping in Electromechanical Waveguides

Yiwei Xia,[1] Emanuele Riva,[2] Matheus I. N. Rosa,[3] Gabriele Cazzulani,[2] Alper Erturk,[1] Francesco Braghin,[2] and Massimo Ruzzene[3]

[1]School of Mechanical Engineering, Georgia Institute of Technology, Atlanta, Georgia 30332, USA
[2]Department of Mechanical Engineering, Politecnico di Milano, 20156 Milano, Italy
[3]Department of Mechanical Engineering, University of Colorado Boulder, Boulder, Colorado 80309, USA

(Received 16 June 2020; accepted 14 January 2021; published 2 March 2021)

We experimentally demonstrate temporal pumping of elastic waves in an electromechanical waveguide. Temporal pumping exploits a virtual dimension mapped to time, enabling the generation and control of edge states, typical of two-dimensional systems, in a one-dimensional waveguide. We show experimentally that the temporal modulation of the stiffness drives the transfer of edge states from one boundary of the waveguide to the other. The considered implementation, that consists of an elastic waveguide coupled with tunable electrical impedances, allows the pumping to occur in a controllable manner. The framework presented herein opens new avenues for the manipulation and transport of information through elastic waves, with potential technological applications for digital delay lines and digitally controlled waveguides. This Letter also explores higher-dimensional topological physics using virtual dimensions mapped to time in electromechanical systems.

DOI: 10.1103/PhysRevLett.126.095501

The transport of information along one-dimensional (1D) waveguides is key to numerous technological applications, but is generally limited by two main factors: (i) fixed propagation speeds and associated wave dispersion that are determined by the properties of the medium and (ii) scattering and localization of the propagating signal at defects and imperfections. The study of topological insulators has opened new pathways to overcome these limitations, sparking broad interest across different realms of physics, including quantum [1], electromagnetic [2,3], acoustic [4–6], and elastic [7] media. Robust waveguiding along edges and interfaces of two-dimensional (2D) domains has been demonstrated in different elastic and acoustic platforms, exploiting analogies with the quantum Hall effect (QHE) [8–16], the quantum spin Hall effect [7,17–21], and the quantum valley Hall effect [22–25]. These works and the references therein illustrate a variety of strategies for robust wave transport, which generally require 2D domains and occur at fixed (nontunable) speeds.

A recent line of work exploits virtual dimensions in parameter space to explore higher-dimensional topological effects in lower-dimensional systems [26–30]. For example, edge states commonly attributed to (2D) QHE systems have been illustrated in 1D periodic [31,32] and quasiperiodic [33–37] systems, while 4D and 6D quantum Hall phases have been observed in 2D [38–40] and 3D [30,41] lattices. In this context, topological pumping emerges as a phenomenon that promotes edge-to-edge transitions of topological states, induced by parametric variations along one additional dimension, either spatial [32,33,38,39,42–44] or temporal [15,45–50]. A temporal pump embodies a 2D topological effect that governs the robust energy transport in systems of a single spatial dimension. While a promising concept supported mostly by theoretical investigations [15,48,50,51], its experimental realization for elastic waves has so far been elusive. Notable recent studies include the temporal pumping illustrated in a dimerized magnetomechanical system emulating the Su-Schreefer-Heeger model [47] and its realization for acoustic lattices [52]. These contributions highlight the potential of temporal pumping for robust wave transport, but further efforts are still required toward implementations in compact and modular configurations, which can be potentially scaled down for on-chip applications.

Among the available physical platforms, continuous waveguides are excellent candidates for this purpose and have been extensively employed as versatile platforms for the realization of phononic circuits with distinct functionalities [21,53,54]. Motivated by these works and by prior works on topological pumping through spatial stiffness modulations in two-dimensional domains [32,43], we pursue temporal pumping of edge states in a 1D continuous system. To this end, we explore a configuration that enables the time modulation of the elastic properties of an electromechanical waveguide, which allows for the control of both magnitude and schedule of the modulations. This behavior was previously illustrated for mechanical systems in pure theoretical studies [32,51] and in discrete systems of limited tunability and modal content [35,47]. Thus, we provide an experimental demonstration of adiabatic temporal pumping for the first time in a continuous waveguide through an experimental setup that is suitable

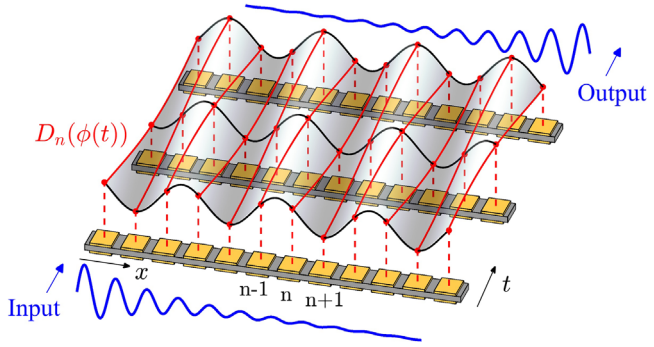

FIG. 1. Concept of temporal pumping implemented in an electromechanical elastic beam. The equivalent stiffness $D_n(\phi)$ at the location of the nth piezoelectric patches (red lines) is obtained by sampling the surface $D(x,\phi) = D_0[1 + \alpha\cos(2\pi\theta x + \phi)]$ at $x_n = n$ [32]. The spatial stiffness modulation with slowly varying temporal phase $\phi(t)$ induces the transition of the left-localized edge state (input) into a right-localized state (output).

for miniaturization and for device-level implementation and constitute a physical platform to study higher-dimensional topological effects in lower-dimensional systems.

We consider an elastic beam (gray solid in Fig. 1) where spatiotemporal modulation is induced by an array of piezoelectric patches (yellow), bonded on the top and bottom surfaces and shunted through negative capacitance (NC) circuits [55]. The NC shunts modify the equivalent bending stiffness D according to the following modulation:

$$D_n(\phi) = D_0[1 + \alpha\cos(2\pi n\theta + \phi)], \tag{1}$$

where D_n is the contribution to the bending stiffness at the location of the nth piezo pair (Fig. 1). This spatial stiffness modulation produces edge states localized at one of the boundaries of the waveguide depending on the assigned value of the modulation phase ϕ [32]. An adiabatic temporal modulation of the phase $\phi(t)$ drives a left-localized edge state (input) across the waveguide, producing a right-localized state (output), thus implementing topological pumping.

Wave motion along the waveguide is predicted by employing Euler-Bernoulli beam theory [56], which describes the transverse harmonic motion at $w(x,\omega)$ of the waveguide through the following governing equation:

$$[D(x)w_{,xx}]_{,xx} = \omega^2 m(x)w(x,\omega), \tag{2}$$

where $[]_{,x}$ denotes a derivative with respect to x, while m is the linear mass of the beam. The stiffness and inertia properties of the waveguide can be expressed as

$$D(x) = D_b + \sum_n D_n H(x - nx_p, l_p), \tag{3}$$

$$m(x) = m_b + \sum_n m_p H(x - nx_p, l_p), \tag{4}$$

where D_n is given in Eq. (1), D_b and m_b, respectively, denote the bending stiffness and linear mass of the base beam, and m_p is the increase in linear mass at the locations of the patches. Also in Eq. (3), $H(\cdot)$ is a unit step function centered at location nx_p and of length l_p.

The parameter θ controls the periodicity of the structure: rational values of the type $\theta = p/q$ produce periodic domains, while irrational θ values result in quasiperiodic or incommensurate domains. For simplicity, we consider a modulation with $\theta = 1/3$ in Eq. (1), resulting in a periodic beam, whose period $L_c = 72$ mm comprises three piezoelectric elements of length $l_p = 22$ mm that are 2 mm apart. Other θ values can also produce edge states that can be used for pumping, as discussed in [32,35,36,50,57]. The variable resistance NC shunts produce a stiffness modulation that is quantified by a value of $\alpha = 0.172$. The estimation of these values is based on the procedures described in Supplemental Material [58], where details about the system geometrical and physical parameters are found.

We first investigate the dispersion properties of the modulated waveguide, which are evaluated by employing a finite element discretization of Eq. (2) and the application of Bloch conditions on a unit cell [67], i.e., $w(\omega, x + L_c) = w(\omega, x)e^{-i\kappa L_c}$, where κ is the wave number. Figure 2(a) depicts two dispersion surfaces as a function of ϕ and $\mu = \kappa L_c$, which are separated by a gap of center frequency close to 9.7 kHz. The inset displays the dispersion $\omega(\mu)$ for $\phi = 0$ and shows five bands. The inset also highlights, through the shaded blue area, the frequency range corresponding to the surfaces shown in the main plot, which focuses primarily on the gap separating the fourth and fifth bands. The consideration of the virtual parameter ϕ augments the dispersion bands to be defined over a two-dimensional torus $[\mu, \phi] \in [0, 2\pi]$, where the Chern number becomes the relevant topological invariant [32,43,68]. Evaluation of the Chern number results in $C_4 = 1$ for the fourth band of Fig. 2(a) (green surface), and $C_1 = 1$, $C_2 = -2$, $C_3 = 1$ for the first three bands not depicted in the figure (see details in the Supplemental Material [58]). Similarly, a label for gap r is assigned by the algebraic sum of the Chern number of the bands below it, i.e., $C_g^{(r)} = \sum_{n=1}^{r} C_n$. The first gap in Fig. 2(a) (shaded gray region) is topologically trivial with $C_g = 0$, while the following gap (shaded red region) is nontrivial with $C_g = 1$. The nonzero label indicates its ability to support an edge state spanning the gap in a finite structure [32,43]. We illustrate this by computing the eigenfrequencies of a finite beam comprising eight unit cells for a total of 24 pair of patches. For simplicity, we consider simply supported boundary conditions, while a more accurate model is introduced in the remainder of the Letter to fit the experimental data. Results are shown in Fig. 2(b), which displays the variation of the eigenfrequencies as a function of ϕ (black lines), superimposed to the bulk bands

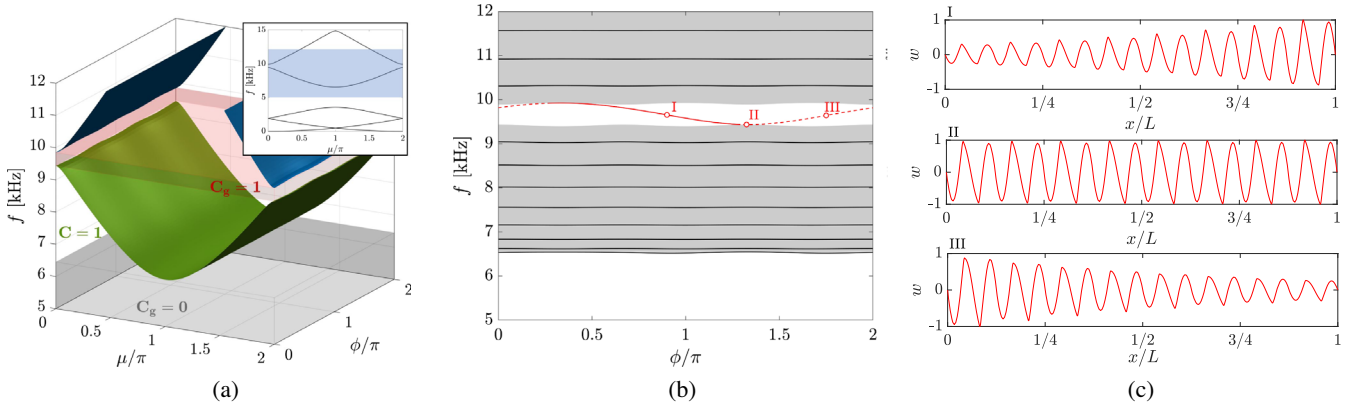

FIG. 2. Dispersion properties and edge states for a beam with equivalent stiffness modulation $D_n(\phi) = D_0[1 + \alpha\cos(2\pi\theta n + \phi)]$. (a) Dispersion surfaces as a function of μ and ϕ with information on Chern numbers and gap labels. The inset displays the first five bands for $\phi = 0$, highlighting the frequency range considered for the surface plot (shaded blue region). (b) Eigenfrequencies for a finite beam as a function of ϕ (black lines) superimposed to the bulk bands (shaded gray regions), where an edge state (red lines) spans the nontrivial gap with $C_g = 1$. (c) States corresponding to the points marked in (b) showing examples of right-localized mode (I), bulk mode (II), and left-localized mode (III).

represented by the shaded gray areas. The additional mode spanning the nontrivial gap is an edge state, where dashed (solid) lines are used for values of ϕ corresponding to left-(right-)localized modes. The three representative modes marked in Fig. 2(b) are displayed in Fig. 2(c) to illustrate a transition of the edge state from right localized (I), to bulk (II), and then to left localized (III) for increasing ϕ values. Such transition is hereafter employed to induce edge-to-edge pumping through a smooth modulation of ϕ in time.

The experimental investigations have as a first goal the characterization of the beam spectrum and its dependence on ϕ. The waveguide is equipped with clamps at both boundaries, which are modeled through the addition of linear and torsional springs [58], and excited at one end by one of the patches. A scanning laser Doppler vibrometer measures the velocity field $\dot{w}(x,t)$ along the beam resulting from a band-limited noise excitation in the 3–15 kHz frequency range. The signal is continuously applied for the duration of the test ($T = 2.2$ s), while the phase ϕ varies in the interval $[0, 2\pi]$. The resulting input and output signals are postprocessed to estimate the frequency response of the beam as a function of the phase ϕ. To this end, the signals are multiplied by a rectangular window of length $T_s = 0.22$ s, centered at an instant t_0, and the frequency response of the beam for $\phi = \phi(t_0)$, i.e., $W(x, \phi(t_0), \omega)$, is obtained by employing an H1 frequency estimator [59]. The center of the window t_0 is smoothly translated in time, while the L_2 norm is taken along the spatial x coordinate. This produces estimations of the frequency response as a function of $\phi(t_0)$, i.e., $W(\phi, \omega)$ [58]. The results are reported as contour plots in Figs. 3(a) and 3(b), which correspond to two experiments where the beam is excited at the left and right boundary, respectively. Black and red lines superimposed to the experimental contours correspond to the eigenfrequencies of the bulk and edge modes predicted numerically. The experimental results show a good agreement with the numerical spectrum: left excitation [Fig. 3(a)] reproduces mostly the left-localized branch of the edge state (dashed lines), while the right excitation experiment [Fig. 3(b)] captures primarily the right-localized branch (solid line). Experimentally measured left- and right-localized modes corresponding to the points marked as I and II in Figs. 3(a) and 3(b) are shown in Fig. 3(c) and compared to the numerical velocity profile.

Upon characterization of the spectrum and corresponding edge states, we next impose the smooth temporal variation of ϕ to induce topological pumping. We first target the left-localized mode defined for $\phi_1 = 1.6\pi$ [mode I in Figs. 3(a) and 3(c)] by applying a harmonic excitation of frequency 9.45 kHz to the left boundary. The excitation signal is maintained for an interval of 12 ms, which is found sufficient to induce the steady-state motion of the left-localized mode and to avoid any contribution of neighboring bulk models. Upon stopping the excitation, we observe the free evolution of the waveguide response as the phase ϕ is varied linearly in time to reach a value of $\phi_2 = 0.4\pi$, which takes approximately 2 ms [Fig. 4(b)]. Figure 4(a) displays the magnitude of the experimentally recorded transverse motion of the beam from $t = 12$ ms onward, i.e., after steady-state conditions are reached. During the displayed time interval, the linear variation of the phase from $\phi_1 = 1.6\pi \rightarrow \phi_2 = 0.4\pi$ induces the expected transition from a left-localized edge state to a right-localized state, as shown in Fig. 4(a). To better illustrate this transition, the recorded response is compensated for dissipation by extracting a temporal decay factor ξ for the edge state at constant ϕ, and then multiplying the transient time history $\dot{w}(x,t)$ by $e^{\xi t}$. Furthermore, the velocity field is normalized by the maximum velocity value measured at the beginning of the pumping process. A comparison with the

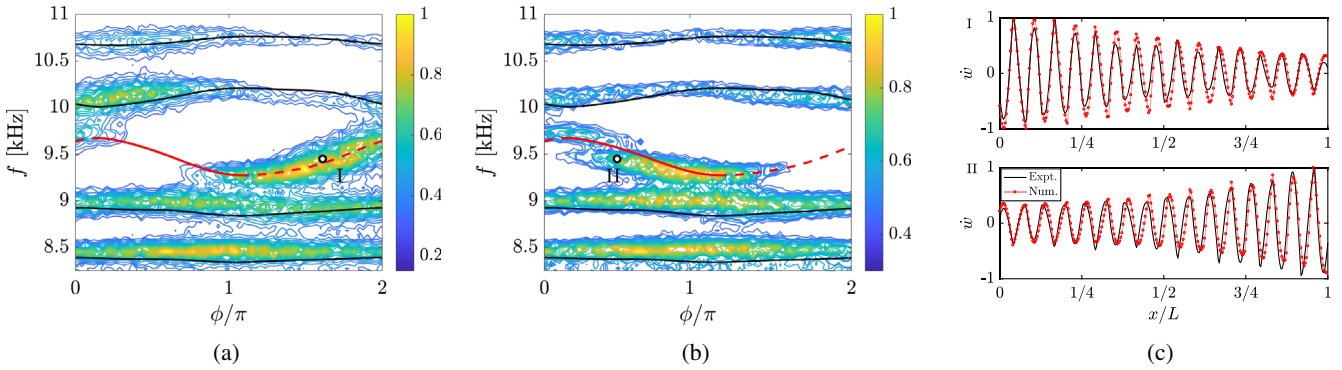

FIG. 3. Experimental spectral characterization of modulated electromechanical beam. (a),(b) Measured frequency response as a function of ϕ (contours) for excitation at the (a) left and (b) right boundary, superimposed to the eigenfrequencies of bulk (black) and edge (red) modes. The left excitation reproduces mostly the left-localized portion of the branch of the edge state (dashed lines), while the right excitation identifies the right-localized portion (solid line). (c) Representative experimental response for left- (I) and right- (II) localized modes. Black and red lines represent experimental and numerical data.

noncompensated diagrams can be found in the Supplemental Material [58]. The procedure does not alter the spatial distribution of the velocity field $\dot{w}$ at any given time instant, but allows for a better visualization of the pump and approximates the behavior of the system should dissipation be minimized. The physical mitigation of dissipation may play an important role in future studies aiming at exploring the full limits of topological pumping, both fast and slow, and can potentially be achieved by introducing a negative loss factor through suitable active circuits [47]. The topological pump displayed in Fig. 4(a) is characterized by an adiabatic [51] transition along the branch of the edge state, as illustrated by the spectral content in Fig. 4(b). In the upper panel, the spectra in Figs. 3(a) and 3(b) are averaged to provide a single spectral characterization of the waveguide and to highlight the presence of an edge state and a bulk mode. The spectrogram in the bottom panel is obtained through the Fourier transformation and appropriate windowing of the transient pump displayed in Fig. 4(a) [58]. The results illustrate how energy remains concentrated around the edge state branch, with negligible contribution to the neighboring bulk modes (black line) as expected in an adiabatic state evolution [51]. We also note that, while the employed experimental setup is subject to variability in its electrical and mechanical parts, the agreement between simulation and experimental results signals a reasonable degree of robustness to defects and imperfections. However, a detailed and quantified analysis on this matter as presented in [47], for example, is a task left for future work, which may be of particular relevance to technological applications requiring a higher degree of accuracy.

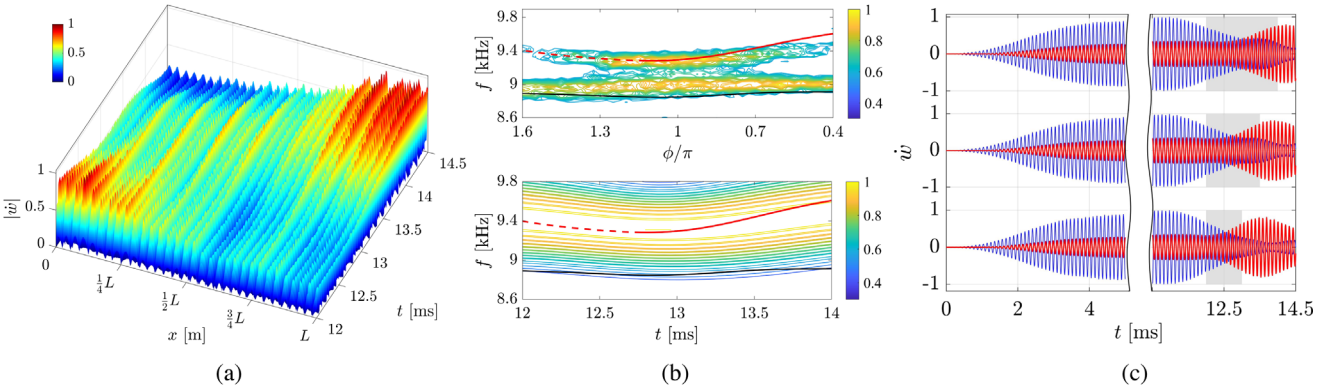

FIG. 4. Experimental demonstration of temporal pumping in the electromechanical waveguide. (a) Transient time history illustrating a transition from a left-localized mode to a right-localized mode, induced by a linear temporal phase variation from $\phi_1 = 1.6\pi \rightarrow \phi_2 = 0.4\pi$ starting at $t = 12$ ms, with a duration of 2 ms. (b) Spectral content of broadband excitation in quasistatic conditions (top) compared to spectrogram of the temporal pump (bottom), illustrating the adiabatic evolution along the branch of the edge state occurring in the pump with negligible influence of the neighboring bulk mode. (c) Signals at left (blue) and right (red) boundaries of the beam for temporal pumps induced within different modulation windows (shaded gray regions). In the initial 12 ms, steady-state vibrations of the left-localized mode are induced (with duration halved for better visualization), while different phase modulation durations (top, 2 ms; middle, 1.5 ms; bottom, 1 ms) delay the arrival of the signal at the right end of the beam.

Finally, we elucidate how the temporal pump realized with controllable phase modulation speeds can be of potential interest for the manipulation and transport of information across the waveguide. Figure 4(c) displays the velocity time history for a point at the left (blue) and right boundary (red) of the beam. The three plots correspond to edge-to-edge transitions driven by different modulation speeds. Under the aforementioned testing conditions, we employed the same input signal, whereby during the first 12 ms a standing left-localized edge state is induced. At $t = 12$ ms, the linear temporal phase modulation $\phi(t)$ starts, ranging from $\phi_1 = 1.6\pi$ to $\phi_2 = 0.4\pi$ during an interval of 1 ms (bottom), 1.5 ms (middle) and 2 ms (top), which are sufficiently away from the limit of adiabaticity $T_{\text{lim}} = 0.67$ ms (see more details in the Supplemental Material [58]). The time duration of the phase modulation is highlighted by shaded gray areas to illustrate how the arrival time of the signal to the right end of the beam (in red) is controlled by the rate of phase modulation. This ability to control the arrival time independently from the underlying properties of the medium (the beam in this case) suggests opportunities for the design of digitally controllable electromechanical delay lines based on topological pumping.

This Letter illustrates an experimental demonstration of temporal pumping in a continuous electromechanical waveguide with controllable modulation capabilities. Such modulations are employed for the topological pumping of edge states according to different modulation rates. This suggests the possibility to implement transfer of information in waveguides at speeds that are uniquely defined by the induced phase modulation and independent of the physical parameters of the host structure. While current limitations associated with bandwidth and controlling the signal shape are noted, these results highlight potential applications to devices relying on robust signal transport, with tunable arrival times and phase delays and open potential pathways for manipulating elastic waves using electromechanical waveguides. This Letter also suggests that elastic structures are convenient platforms for fundamental studies on higher-dimensional topological effects by using virtual dimensions (the phase ϕ in this Letter) mapped to time. For example, 2D platelike domains with time-modulation capabilities provided by piezoelectric patches can be employed in future studies to explore 4D quantum Hall physics where two virtual parameters can be mapped to time [38,40].

The authors gratefully acknowledge the support from the National Science Foundation (NSF) through the EFRI 1741685 grant and from the Army Research office through Grant No. W911NF-18-1-0036. The Italian Ministry of Education, University and Research is acknowledged for the support provided through the Project "Department of Excellence LIS4.0—Lightweight and Smart Structures for Industry 4.0."

[1] M. Z. Hasan and C. L. Kane, Colloquium: Topological insulators, Rev. Mod. Phys. **82**, 3045 (2010).
[2] L. Lu, J. D. Joannopoulos, and M. Soljačić, Topological photonics, Nat. Photonics **8**, 821 (2014).
[3] A. B. Khanikaev, S. H. Mousavi, W.-K. Tse, M. Kargarian, A. H. MacDonald, and G. Shvets, Photonic topological insulators, Nat. Mater. **12**, 233 (2013).
[4] Z. Yang, F. Gao, X. Shi, X. Lin, Z. Gao, Y. Chong, and B. Zhang, Topological Acoustics, Phys. Rev. Lett. **114**, 114301 (2015).
[5] R. Fleury, A. B. Khanikaev, and A. Alu, Floquet topological insulators for sound, Nat. Commun. **7**, 11744 (2016).
[6] J. Lu, C. Qiu, L. Ye, X. Fan, M. Ke, F. Zhang, and Z. Liu, Observation of topological valley transport of sound in sonic crystals, Nat. Phys. **13**, 369 (2017).
[7] S. H. Mousavi, A. B. Khanikaev, and Z. Wang, Topologically protected elastic waves in phononic metamaterials, Nat. Commun. **6**, 8682 (2015).
[8] K. v. Klitzing, G. Dorda, and M. Pepper, New Method for High-Accuracy Determination of the Fine-Structure Constant Based on Quantized Hall Resistance, Phys. Rev. Lett. **45**, 494 (1980).
[9] D. J. Thouless, M. Kohmoto, M. P. Nightingale, and M. den Nijs, Quantized Hall Conductance in a Two-Dimensional Periodic Potential, Phys. Rev. Lett. **49**, 405 (1982).
[10] E. Prodan and C. Prodan, Topological Phonon Modes and Their Role in Dynamic Instability of Microtubules, Phys. Rev. Lett. **103**, 248101 (2009).
[11] P. Wang, L. Lu, and K. Bertoldi, Topological Phononic Crystals with One-Way Elastic Edge Waves, Phys. Rev. Lett. **115**, 104302 (2015).
[12] L. M. Nash, D. Kleckner, A. Read, V. Vitelli, A. M. Turner, and W. T. Irvine, Topological mechanics of gyroscopic metamaterials, Proc. Natl. Acad. Sci. U.S.A. **112**, 14495 (2015).
[13] A. Souslov, B. C. Van Zuiden, D. Bartolo, and V. Vitelli, Topological sound in active-liquid metamaterials, Nat. Phys. **13**, 1091 (2017).
[14] N. P. Mitchell, L. M. Nash, D. Hexner, A. M. Turner, and W. T. Irvine, Amorphous topological insulators constructed from random point sets, Nat. Phys. **14**, 380 (2018).
[15] H. Chen, L. Yao, H. Nassar, and G. Huang, Mechanical Quantum Hall Effect in Time-Modulated Elastic Materials, Phys. Rev. Applied **11**, 044029 (2019).
[16] D. Thouless, Quantization of particle transport, Phys. Rev. B **27**, 6083 (1983).
[17] R. Süsstrunk and S. D. Huber, Observation of phononic helical edge states in a mechanical topological insulator, Science **349**, 47 (2015).
[18] R. K. Pal, M. Schaeffer, and M. Ruzzene, Helical edge states and topological phase transitions in phononic systems using bi-layered lattices, J. Appl. Phys. **119**, 084305 (2016).
[19] H. Chen, H. Nassar, A. N. Norris, G. K. Hu, and G. L. Huang, Elastic quantum spin Hall effect in kagome lattices, Phys. Rev. B **98**, 094302 (2018).
[20] R. Chaunsali, C.-W. Chen, and J. Yang, Subwavelength and directional control of flexural waves in zone-folding induced topological plates, Phys. Rev. B **97**, 054307 (2018).
[21] M. Miniaci, R. K. Pal, B. Morvan, and M. Ruzzene, Experimental Observation of Topologically Protected

Helical Edge Modes in Patterned Elastic Plates, Phys. Rev. X **8**, 031074 (2018).
[22] R. K. Pal and M. Ruzzene, Edge waves in plates with resonators: An elastic analogue of the quantum valley Hall effect, New J. Phys. **19**, 025001 (2017).
[23] J. Vila, R. K. Pal, and M. Ruzzene, Observation of topological valley modes in an elastic hexagonal lattice, Phys. Rev. B **96**, 134307 (2017).
[24] T.-W. Liu and F. Semperlotti, Tunable Acoustic Valley-Hall Edge States in Reconfigurable Phononic Elastic Waveguides, Phys. Rev. Applied **9**, 014001 (2018).
[25] T.-W. Liu and F. Semperlotti, Experimental Evidence of Robust Acoustic Valley Hall Edge States in a Nonresonant Topological Elastic Waveguide, Phys. Rev. Applied **11**, 014040 (2019).
[26] X.-L. Qi, T. L. Hughes, and S.-C. Zhang, Topological field theory of time-reversal invariant insulators, Phys. Rev. B **78**, 195424 (2008).
[27] Y. E. Kraus and O. Zilberberg, Quasiperiodicity and topology transcend dimensions, Nat. Phys. **12**, 624 (2016).
[28] E. Prodan, Virtual topological insulators with real quantized physics, Phys. Rev. B **91**, 245104 (2015).
[29] T. Ozawa, H. M. Price, N. Goldman, O. Zilberberg, and I. Carusotto, Synthetic dimensions in integrated photonics: From optical isolation to four-dimensional quantum Hall physics, Phys. Rev. A **93**, 043827 (2016).
[30] C. H. Lee, Y. Wang, Y. Chen, and X. Zhang, Electromagnetic response of quantum Hall systems in dimensions five and six and beyond, Phys. Rev. B **98**, 094434 (2018).
[31] V. M. Alvarez and M. Coutinho-Filho, Edge states in trimer lattices, Phys. Rev. A **99**, 013833 (2019).
[32] M. I. Rosa, R. K. Pal, J. R. Arruda, and M. Ruzzene, Edge states and Topological Pumping in Spatially Modulated Elastic Lattices, Phys. Rev. Lett. **123**, 034301 (2019).
[33] Y. E. Kraus, Y. Lahini, Z. Ringel, M. Verbin, and O. Zilberberg, Topological States and Adiabatic Pumping in Quasicrystals, Phys. Rev. Lett. **109**, 106402 (2012).
[34] D. J. Apigo, W. Cheng, K. F. Dobiszewski, E. Prodan, and C. Prodan, Observation of Topological Edge Modes in a Quasiperiodic Acoustic Waveguide, Phys. Rev. Lett. **122**, 095501 (2019).
[35] X. Ni, K. Chen, M. Weiner, D. J. Apigo, C. Prodan, A. Alù, E. Prodan, and A. B. Khanikaev, Observation of Hofstadter butterfly and topological edge states in reconfigurable quasiperiodic acoustic crystals, Commun. Phys. **2**, 55 (2019).
[36] R. K. Pal, M. I. N. Rosa, and M. Ruzzene, Topological bands and localized vibration modes in quasiperiodic beams, New J. Phys. **21**, 093017 (2019).
[37] Y. Xia, A. Erturk, and M. Ruzzene, Topological Edge States in Quasiperiodic Locally Resonant Metastructures, Phys. Rev. Applied **13**, 014023 (2020).
[38] O. Zilberberg, S. Huang, J. Guglielmon, M. Wang, K. P. Chen, Y. E. Kraus, and M. C. Rechtsman, Photonic topological boundary pumping as a probe of 4D quantum Hall physics, Nature (London) **553**, 59 (2018).
[39] M. Lohse, C. Schweizer, H. M. Price, O. Zilberberg, and I. Bloch, Exploring 4d quantum Hall physics with a 2d topological charge pump, Nature (London) **553**, 55 (2018).
[40] M. Rosa, M. Ruzzene, and E. Prodan, Topological gaps by twisting, arXiv:2006.10019.
[41] I. Petrides, H. M. Price, and O. Zilberberg, Six-dimensional quantum Hall effect and three-dimensional topological pumps, Phys. Rev. B **98**, 125431 (2018).
[42] M. Verbin, O. Zilberberg, Y. Lahini, Y. E. Kraus, and Y. Silberberg, Topological pumping over a photonic Fibonacci quasicrystal, Phys. Rev. B **91**, 064201 (2015).
[43] E. Riva, M. I. Rosa, and M. Ruzzene, Edge states and topological pumping in stiffness-modulated elastic plates, Phys. Rev. B **101**, 094307 (2020).
[44] Z.-G. Chen, W. Tang, R.-Y. Zhang, and G. Ma, Landau-Zener Transition in the Dynamic Transfer of Acoustic Topological States, Phys. Rev. Lett. **126**, 054301 (2021)..
[45] S. Nakajima, T. Tomita, S. Taie, T. Ichinose, H. Ozawa, L. Wang, M. Troyer, and Y. Takahashi, Topological Thouless pumping of ultracold fermions, Nat. Phys. **12**, 296 (2016).
[46] M. Lohse, C. Schweizer, O. Zilberberg, M. Aidelsburger, and I. Bloch, A Thouless quantum pump with ultracold bosonic atoms in an optical superlattice, Nat. Phys. **12**, 350 (2016).
[47] I. H. Grinberg, M. Lin, C. Harris, W. A. Benalcazar, C. W. Peterson, T. L. Hughes, and G. Bahl, Robust temporal pumping in a magneto-mechanical topological insulator, Nat. Commun. **11**, 974 (2020).
[48] I. Brouzos, I. Kiorpelidis, F. Diakonos, and G. Theocharis, Non-adiabatic time-optimal edge mode transfer on mechanical topological chain, Phys. Rev. B **102**, 174312 (2020).
[49] S. Longhi, Topological pumping of edge states via adiabatic passage, Phys. Rev. B **99**, 155150 (2019).
[50] E. Riva, V. Casieri, F. Resta, and F. Braghin, Adiabatic pumping via avoided crossings in stiffness-modulated quasiperiodic beams, Phys. Rev. B **102**, 014305 (2020).
[51] H. Nassar, H. Chen, A. Norris, and G. Huang, Quantization of band tilting in modulated phononic crystals, Phys. Rev. B **97**, 014305 (2018).
[52] W. Cheng, E. Prodan, and C. Prodan, Demonstration of Dynamic Topological Pumping across Incommensurate Acoustic Meta-Crystals, Phys. Rev. Lett. **125**, 224301 (2020).
[53] T.-W. Liu and F. Semperlotti, Tunable Acoustic Valley–Hall Edge States in Reconfigurable Phononic Elastic Waveguides, Phys. Rev. Applied **9**, 014001 (2018).
[54] J. Vila, R. K. Pal, and M. Ruzzene, Observation of topological valley modes in an elastic hexagonal lattice, Phys. Rev. B **96**, 134307 (2017).
[55] J. Marconi, E. Riva, M. Di Ronco, G. Cazzulani, F. Braghin, and M. Ruzzene, Experimental Observation of Nonreciprocal Band Gaps in a Space-Time-Modulated Beam Using a Shunted Piezoelectric Array, Phys. Rev. Applied **13**, 031001(R) (2020).
[56] K. F. Graff, *Wave Motion in Elastic Solids* (Courier Corporation, New York, 2012).
[57] E. Prodan and Y. Shmalo, The *k*-theoretic bulk-boundary principle for dynamically patterned resonators, J. Geom. Phys. **135**, 135 (2019).
[58] See Supplemental Material at http://link.aps.org/supplemental/10.1103/PhysRevLett.126.095501 for more details on the simulation procedures, experimental setup, and methodology, which includes Refs. [59–66].
[59] K. Worden, *Nonlinearity in Structural Dynamics: Detection, Identification and Modelling* (CRC Press, Boca Raton, FL, 2019).

[60] O. C. Zienkiewicz and R. L. Taylor, *The Finite Element Method for Solid and Structural Mechanics* (Elsevier, New York, 2005).

[61] T. Fukui, Y. Hatsugai, and H. Suzuki, Chern numbers in discretized Brillouin zone: Efficient method of computing (spin) Hall conductances, J. Phys. Soc. Jpn. **74**, 1674 (2005).

[62] S. Ibáñez and J. Muga, Adiabaticity condition for non-Hermitian Hamiltonians, Phys. Rev. A **89**, 033403 (2014).

[63] D. Tong, Quantitative Condition is Necessary in Guaranteeing the Validity of the Adiabatic Approximation, Phys. Rev. Lett. **104**, 120401 (2010).

[64] M. H. Amin, Consistency of the Adiabatic Theorem, Phys. Rev. Lett. **102**, 220401 (2009).

[65] V. Yukalov, Adiabatic theorems for linear and nonlinear Hamiltonians, Phys. Rev. A **79**, 052117 (2009).

[66] X. Yi, D. Tong, L. Kwek, and C. Oh, Adiabatic approximation in open systems: An alternative approach, J. Phys. B **40**, 281 (2007).

[67] M. I. Hussein, M. J. Leamy, and M. Ruzzene, Dynamics of phononic materials and structures: Historical origins, recent progress, and future outlook, Appl. Mech. Rev. **66**, 040802 (2014).

[68] Y. Hatsugai, Chern Number and Edge States in the Integer Quantum Hall Effect, Phys. Rev. Lett. **71**, 3697 (1993).